Pergamon

Int. J. Mach. Tools Manufact. Vol. 34, No. 6, pp. 879–891, 1994
Elsevier Science Ltd
Printed in Great Britain
0890-6955/94$7.00 + .00

CAD ASSISTED CHATTER-FREE NC TOOL PATH GENERATION IN MILLING

M. WECK,† Y. ALTINTAS‡ AND C. BEER†

(*Received* 17 *March* 1993)

Abstract—A chatter vibration-free NC tool path preparation strategy is presented for CAD/CAM systems. The stability charts, which contain chatter-free axial depth and radial width of cuts at a practical cutting speed range, are identified from time domain simulation of dynamic end milling operations. The time domain simulation system allows multiple modes of the machine tool–end mill structure whose transfer functions are measured. The existing pocketing routines in a CAD/CAM system are corrected by planning chatter-free axial depth and radial width of cuts that are automatically selected from the stability data bank during NC tool path generation. A newly introduced linear tool-path pocketing strategy is shown to be the most productive algorithm for dynamically corrected tool paths. The method is supported by experimental results.

NOMENCLATURE

a_e	radial width of cut
b	axial depth of cut
D	cutter diameter
D_k	modal damping factor for the kth mode
d_{iFj}	directional factors in the i and j directions
$F_{x,v,w}, F_{y,v,w}$	cutting forces in the x and y directions, (v) disc element, (w) helical flute
f_z	feed per tooth
G_{Fij}	transfer functions in the i and j directions
h	chip thickness
i	discrete time counter
k_{cb}	linear cutting force coefficient
L	gauge length of the cutter
n	cutting speed
r	number of cutting discs
S_k	modal flexibility for the kth mode
T_t	tooth passing period
t	time
x,y	displacements in x and y direction
z	number of teeth
β	cutting force angle
φ	angle of the cutting tooth position
λ	helix angle
$\Delta\lambda$	angular increment between two segments of the cutting blade
ω_{0k}	natural frequency of the kth mode

1. INTRODUCTION

THE PRESENCE of chatter vibrations in machining operations lead to poor surface finish, chipping of cutting tools, and even damage to the machine tool. There has been a significant amount of research in modelling and analysis of chatter vibrations [1, 2]. The recent research is mostly concentrated on the suppression of chatter vibrations with on-line and off-line techniques.

It is known that the chatter vibrations occur when there is a dynamic flexibility between tool and workpiece, and when the magnitudes of axial and radial depth of

†Laboratory for Machine Tools and Production Engineering (WZL), University of Aachen (RWTH), F.R.G.

‡Visiting Professor on Alexander von Humboldt Research Fellowship to the WZL, University of British Columbia, Vancouver, B.C., Canada.

cuts are larger than critical stability limits. The chatter reduces at low speeds owing to process damping, and generally increases at high cutting speeds where the process damping is negligible [2]. However, at high cutting speeds, favourable stability pockets are close to the dominant natural mode of the structure and its sub-harmonics. All the chatter suppression techniques presented in the literature use one or more of the physical features summarized above.

On-line chatter suppression techniques either manipulate the cutting speed or reduce the process gain, i.e. axial or radial depth of cuts, in milling. Weck *et al.* [3, 4] detected the chatter on-line and continuously reduced the depth of cut until the chatter diminishes. The radial or axial depth of cuts are automatically distributed on-line using the method. Altintas and Chan [5] showed that when the spindle speed is continuously varied, the phase between inner and outer modulations of the chip is disturbed, which leads to a slight improvement of stability. Recently, Smith and Tlusty [6] presented a method of suppressing chatter at high speed milling operations. By matching the tooth passing frequency, i.e. cutting force excitation, with the chatter frequency, they move the machining process to the most favourable stability lobe where larger axial or radial depth of cuts can be removed without chatter vibrations.

There are off-line alternatives to the on-line suppression of chatter that require robust detection of vibrations during machining. The most common method is to prepare the stability charts from machining experiments, and select the chatter-free cutting speed, axial and radial depth of cuts accordingly. However, a considerable number of cutting tests is required to setup the stability charts experimentally. Tlusty and Ismail [7] introduced time domain simulation models for chatter. Because the chatter vibration expressions are non-linear differential equations due to a regeneration mechanism, a reliable analytical solution is not possible. Montgomery and Altintas [8] presented an improved time domain chatter simulation where the chip thickness, contact stiffness and process damping are accounted for more accurately. In general, the time domain chatter simulation algorithms are quite reliable in predicting the axial and radial depth of cuts provided that the cutting stiffness and process damping are selected accurately.

It has been common practice to generate NC tool paths on CAD/CAM systems where the part geometry and tool path are known. Weck *et al.* [9] have integrated the machining technology data to CATIA CAD/CAM system in order to assist NC programmers for suitable cutting speed, feed and tool selection for a given material. Altintas and Spence [10] integrated the mechanics of milling to NC tool path generation in solid model-based CAD/CAM systems. Their system can predict the cutting forces, torque and dimensional form errors left on the finished surface. Tlusty and Smith [11, 12] extended the use of time-domain chatter simulation for chatter-free planning of NC tool paths in CAD/CAM systems. They have automatically selected axial and radial depth of cuts from stability charts prepared by simulations and experiments. A similar strategy is followed in this paper. A comprehensive time domain milling simulation strategy is developed for multi-degree-of-freedom structures including cross-influence of transfer functions [13, 14]. The simulated stability charts are experimentally verified, and used to generate matrices of chatter-free axial depth and radial width of cuts at different speeds. In order to discard the influence of process damping, a high cutting speed region is selected, which is the present trend in high speed machining. The pocketing routines in a commercial CATIA system are modified so that most acceptable, chatter-free, optimal radial width and axial depth of cuts, and cutting directions are selected. Furthermore, a new pocketing strategy is introduced that is proven to produce higher chatter-free material removal rates than the present routines.

Henceforth, the paper is organized as follows. In Section 2, a time-domain simulation model for helical end milling is presented. The preparation of stability chart and its use in NC tool path generation are presented in Section 3. The paper is concluded with a brief summary of the developed system.

2. MODELLING OF CHATTER VIBRATIONS IN HELICAL END MILLS

The geometry of helical end milling is shown in Fig. 1 for a three-fluted cutter that is divided into r number of differential elements in the axial direction in order to account for the helix angle (λ). Each axial cutting edge segment, which has a length of ($\Delta b = b/r$), removes sinusoidally varying chip thicknesses ($f_z \sin(\pi/2\text{-}\varphi_{v,w})$) as the tool rotates without any vibration. The resultant cutting force produced by each differential cutter disc is:

$$F_{v,w} = k_{cb}\,\Delta b\, f_z \sin\left(\frac{\pi}{2} - \varphi_{v,w}\right) \tag{1}$$

where k_{cb} is the linear cutting force coefficient identified from a set of milling experiments [4]. The position angle of a cutting point, $\varphi_{v,w}$ is shown in Fig. 1. The end mill structure bends statically under the quasi-static cutting forces given above, and the static chip deformations are not considered in the simulation of dynamic milling for simplicity. When the end mill vibrates, a cutting edge element leaves an oscillatory surface behind, which is removed by the following vibrating edge. Thus, the chip dynamically varies from its intended static thickness, and produces proportional dynamic cutting forces that are considered here for the stability table preparation. The dynamic resultant cutting force produced by a disc element (v) of a helical flute (w) which has an angular position ($\varphi_{v,w}$) is given by:

$$F_{v,w} = k_{cb}\,\Delta b[h(t) - h(t - T)] \tag{2}$$

where $h(t)$ and $h(t - T)$ are the variations in the chip thickness from its static value, and caused by the vibrations of the element towards the cutter centre at time t and previous tooth period ($t - T$). During cutting, the edge segment may jump out of cut and produces zero force at that instant. This is the basic non-linearity in chatter [7], and considered in the time-domain chatter simulation presented here. Furthermore, in order to calculate the dynamic chip thickness correctly, the vibration marks left in the three previous tooth periods are considered in the simulation program. The resulting dynamic chip thickness $h(t)$ at time t is calculated from dynamic displacements in the feed (x) and normal (y) directions (see Fig. 1):

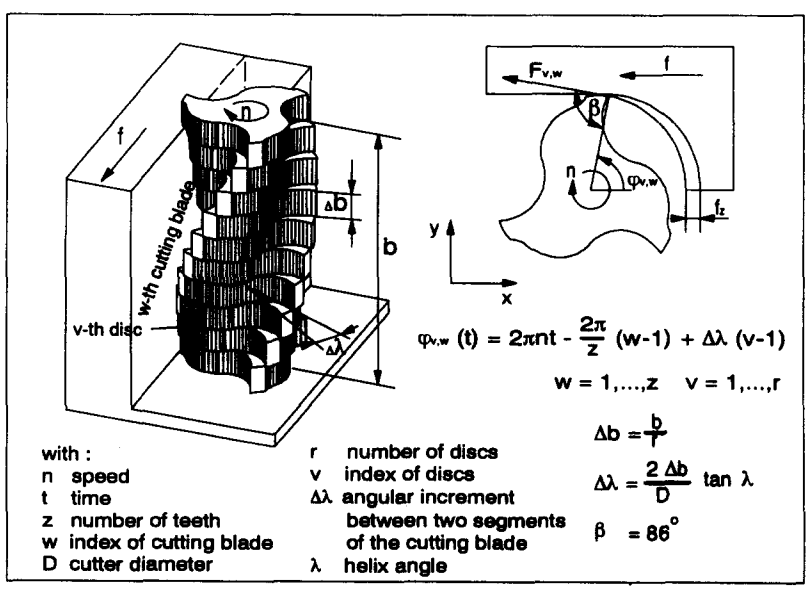

FIG. 1. Model of the helical end mill.

$$h(t) = x\cos(\varphi_{v,w}) + y\sin(\varphi_{v,w}) \; . \tag{3}$$

The dynamic cutting force makes a constant angle, β, with the tool centre, and its components in the x and y directions are resolved from Fig. 1 as:

$$\begin{aligned} F_{x,v,w}(t) &= -k_{cb}\, b[d_{xF_x}(x(t) - x(t - T_t)) + d_{yF_x}(y(t) - y(t - T_t))] \\ F_{y,v,w}(t) &= -k_{cb}\, b[d_{xF_y}(x(t) - x(t - T_t)) + d_{yF_y}(y(t) - y(t - T_t))] \end{aligned} \tag{4}$$

where the geometric directional factors are lumped into the following parameters [4]:

$$\begin{aligned} d_{xF_x} &= \cos\varphi_{v,w}\cos\lambda\cos(\varphi_{v,w} - \beta) \\ d_{yF_x} &= \sin\varphi_{v,w}\cos\lambda\cos(\varphi_{v,w} - \beta) \\ d_{xF_y} &= \cos\varphi_{v,w}\cos\lambda\sin(\varphi_{v,w} - \beta) \\ d_{yF_y} &= \sin\varphi_{v,w}\cos\lambda\sin(\varphi_{v,w} - \beta) \; . \end{aligned} \tag{5}$$

It is assumed that the structural dynamics of the end mill clamped in the tool holder are lumped close to the free end of the tool, and do not change along the axial depth of cut. The cutting forces in feed (F_x) and normal (F_y) directions bend the helical end mill in the plane of cut, and they modulate the chip thickness during dynamic cutting or *chatter*. The equation of vibration for the end mill can be expressed as:

$$\begin{bmatrix} x \\ y \end{bmatrix} = \begin{bmatrix} G_{F_{xx}} & G_{F_{yx}} \\ G_{F_{xy}} & G_{F_{yy}} \end{bmatrix} \begin{bmatrix} F_x \\ F_y \end{bmatrix} \tag{6}$$

where $G_{F_{xx}}$ and $G_{F_{yy}}$ are the direct transfer functions for the structure in the feed and normal directions, respectively. $G_{F_{xy}}$ and $G_{F_{yx}}$ are the cross-transfer functions, and they are usually identical in most spindle systems. The transfer functions for the slender end mill clamped in the tool holder are identified experimentally using a standard modal analysis technique [15] in the frequency domain and is given as:

$$G(j\omega) = \frac{x}{F_x} = \sum_{k=1}^{n} \frac{S_k}{1 - \left(\dfrac{\omega}{\omega_{0k}}\right)^2 + 2jD_k\dfrac{\omega}{\omega_{0k}}} \tag{7}$$

where D_k, ω_{0k}, and S_k are the modal damping factor, natural frequency and modal flexibility for the kth mode, respectively. The time domain equation of motion in the x direction contributed by the direct transfer function, G_{xx}, for mode k can be expressed as:

$$x_k(t) + \frac{2D_k}{\omega_{0k}}\frac{\mathrm{d}x_k(t)}{\mathrm{d}t} + \frac{1}{\omega_{0k}^2}\frac{\mathrm{d}^2x_k(t)}{\mathrm{d}t^2} = S_kF_x(t) \; . \tag{8}$$

In dynamic milling, the above differential equation is solved numerically at small time steps, Δt, which is selected ten times smaller than the period of the highest natural mode in the simulation system. The following Euler method is used for the numerical integration:

$$\frac{dx_k(t)}{dt} \Rightarrow \frac{x_{k,i} - x_{k,i-1}}{\Delta t}$$

$$\frac{d^2x_k(t)}{dt^2} \Rightarrow \frac{x_{k,i+1} - 2x_{k,i} + x_{k,i-1}}{\Delta t^2}$$

$$x_{k,i} + \frac{2D_k}{\omega_{0k}\Delta t}(x_{k,i} - x_{k,i-1}) + \frac{1}{\omega_{0k}^2 \Delta t^2}(x_{k,i+1} - 2x_{k,i} + x_{k,i-1}) = S_k F_i$$

$$x_{k,i+1} = \omega_{0k}^2 \Delta_t^2 \left[S_k F_i - \left(1 + \frac{2D_k}{\omega_{0k}\Delta t} - \frac{2}{\omega_{0k}^2 \Delta t^2}\right) x_{k,i} - \left(\frac{1}{\omega_{0k}^2 \Delta t^2} - \frac{2D_k}{\omega_{0k}\Delta t}\right) x_{k,i-1} \right] \quad (9)$$

where i is the discrete time counter, i.e. $t_i = i\,\Delta t$.

The dynamic displacements are calculated from direct and cross-transfer functions for each mode (k) and summed to calculate the complete displacements for (n) modes:

$$x_{i+1} = \sum_{k=1}^{n} x_{x,i+1} + \sum_{k=1}^{n} x_{y,i+1}$$

$$y_{i+1} = \sum_{k=1}^{n} y_{x,i+1} + \sum_{k=1}^{n} y_{y,i+1} \,. \quad (10)$$

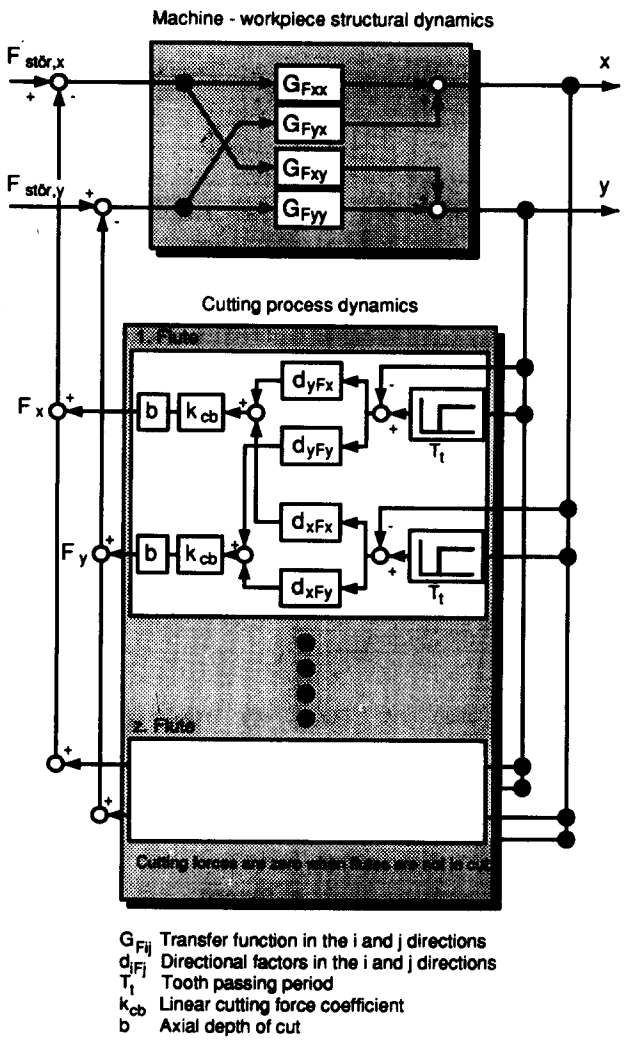

FIG. 2. Time domain simulation for chatter in end milling.

The simulation block diagram for chatter vibrations are shown in Fig. 2. The simulation strategy is similar to the methods presented earlier by Tlusty and Ismail [7].

The correctness of the chatter simulation system is verified experimentally using the measured transfer functions of an end mill attached to the spindle of a Maho CNC machining centre. The structure has one dominant mode in each direction (x,y), and its measured direct transfer functions are given in Fig. 3. The cross-transfer functions had negligible strengths in this particular structure. The cutting coefficient for the aluminium material used is $k_{cb} = 600\ \text{N/mm}^2$. A three-fluted helical end mill with $\lambda = 30°$ helix angle and measured cutting force angle of $\beta = 86°$ is used. The dynamic milling is simulated for slot milling with depths of cut $b = 1$ and 2 mm. Sample displacement history in the x direction shows that the process is unstable for $b = 2$ mm due to continuously growing vibration amplitudes (see Fig. 4). The simulation algorithm assumes that the process is unstable when the peak values of the vibration grow in thirty consecutive oscillation periods, otherwise the process is assumed to be stable.

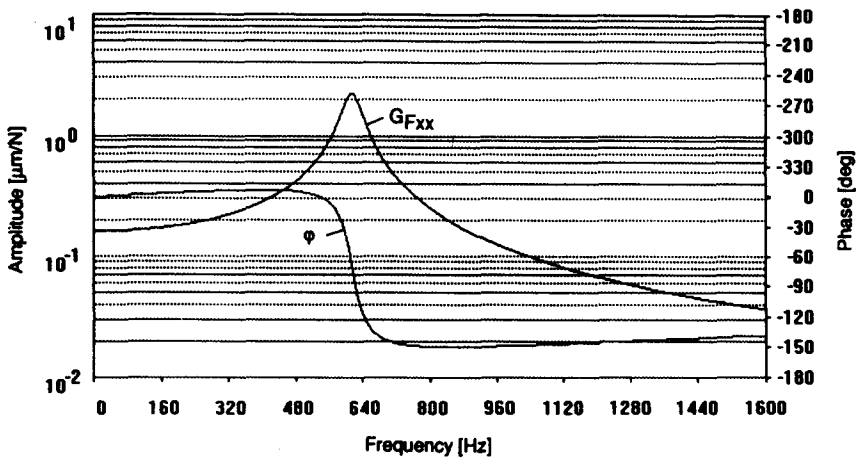

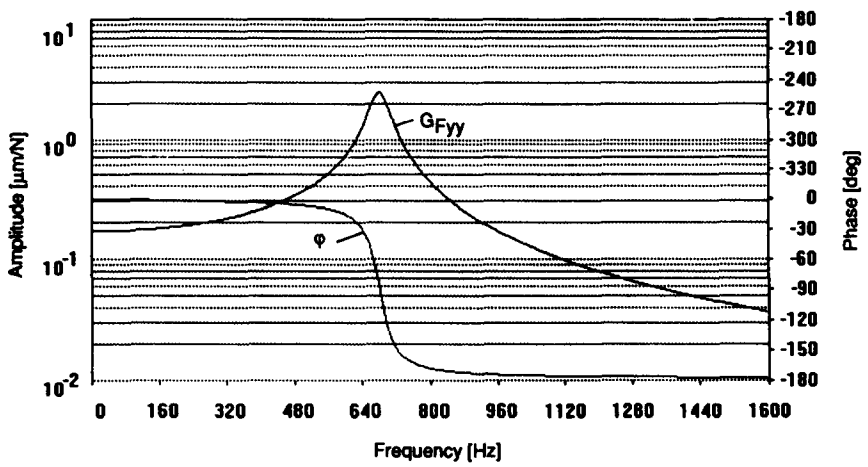

Modes	Frequency f_k [Hz]	Damping D_k [%]	Modal Flexibility S_k [µm/N]
G_{Fxx}	602.9	3.9	0.179
G_{Fyy}	666.2	3.5	0.175

FIG. 3. Measured transfer function and identified modal parameter of the machine with an end mill ($D = 30$ mm; $L = 110$ mm).

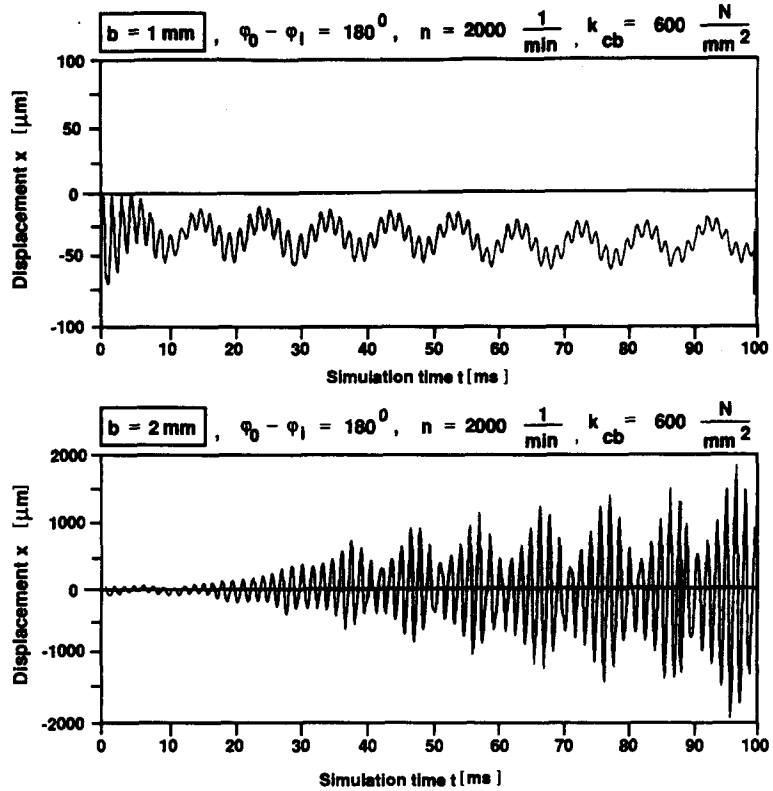

FIG. 4. Stable and unstable machining with an end mill.

The stability of the milling process is simulated under different cutting speeds, v_c, axial depth, b, and radial width, a_e, of cuts, and stable and unstable regions are identified. Sample stability charts (i.e. lobes), identified from milling experiments and simulations, are shown in Fig. 5. The experiments are conducted above 100 m/min cutting speed, where the process damping influence is negligible [2]. The small circles represent the experimental observations, and the continuous curve is the stability lobe generated by

TABLE 1. PRINCIPLE OF MACHINING TECHNOLOGY DATA BANK (SEE FIG. 3 FOR THE TRANSFER FUNCTIONS OF THE MACHINE TOOL)

Machine tool:	Maho 700S
Cutter:	HSS-Endmill D = 30 mm; L = 65 mm; z = 3
Workpiece material:	AlZnMgCu 1,5
Down- or Up-milling:	Up-milling
Spindle speed:	n = 3000/min

Axial depth b (mm)	Radial width of cut a_e(mm) Feed direction in x–y machine coordinate system									
	0°	10°	20°	30°	40°	50°	60°	70°	80°	90°
1	30	30	30	30	30	30	30	29	28	28
2	30	30	30	30	29	28	26	25	22	20
3	30	30	29	27	26	24	22	19	17	14
4	29	28	27	25	23	21	20	16	13	10
5	28	26	25	22	20	17	15	12	10	7
6	27	25	23	21	18	16	13	10	8	6
7	26	24	21	19	16	14	11	9	6	4
8	24	22	20	17	15	12	10	7	5	3
9	24	22	19	17	14	12	9	7	5	3
10	22	19	17	14	12	9	7	5	3	1

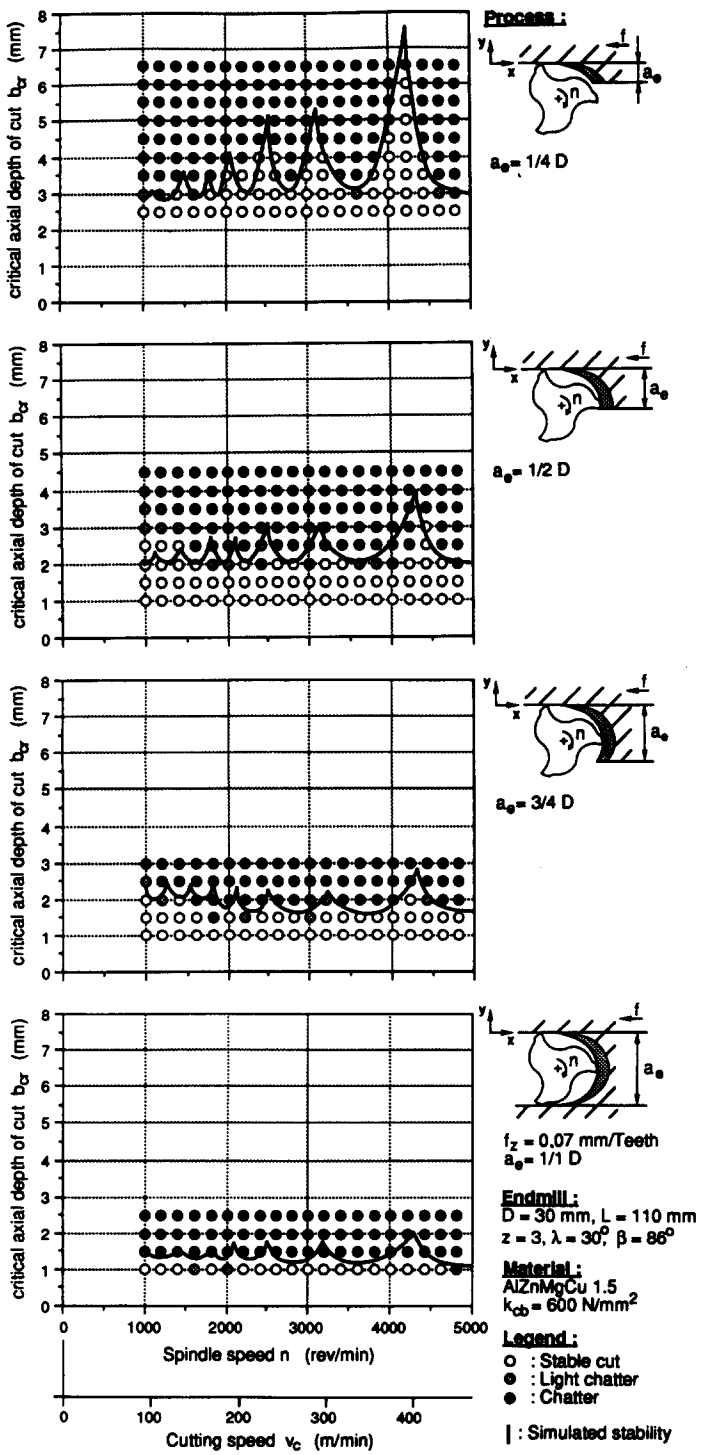

FIG. 5. Simulated stability lobes for an end mill.

the simulation system. The agreement between the experimental and simulation results is satisfactory as can be seen in Fig. 5.

Upon the experimental verification of the chatter simulation systems, a stability data table is constructed for the Maho machine with a three-fluted end mill having a diameter of $D = 30$ mm and a gauge length of $L = 65$ mm. The stability table is constructed for different axial and radial depths, and cutting directions. A sample stability table

for one cutting speed is shown in Table 1. The stability data banks are prepared by the simulation program running on a personal computer, and sent to the database of a CATIA CAD/CAM system via a computer network.

3. CHATTER-FREE NC TOOL PATH PLANNING STRATEGY IN CAD/CAM SYSTEMS

The most common and time consuming process in end milling is the pocketing operation. In general, the NC programs for pocket machining are generated in CAD/CAM systems using standard pocketing routines. As indicated by Tlusty and Smith [11], the present *conventional* pocketing routines in commercial CAD/CAM systems do not consider the process physics, and they are totally based on the correctness of the tool path coordinates. However, randomly selected radial width and axial depth of cuts may produce severe chatter vibrations that lead to unacceptable surface finish

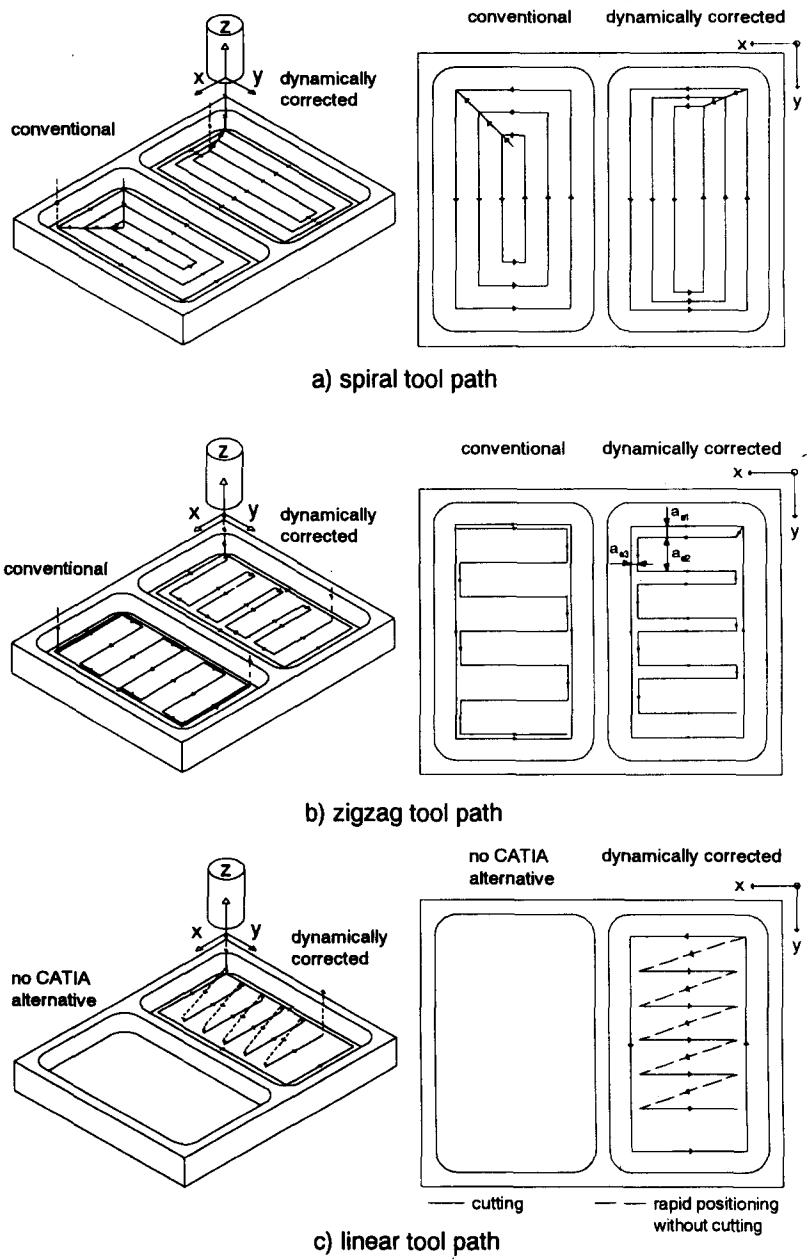

FIG. 6. Conventional and dynamically corrected tool path for pocketing.

and tool failures. The stability of a milling system depends on the transfer functions of the structure, workpiece material, tool geometry and cutting conditions as explained above, and they must be considered during tool path generation in CAD/CAM systems. Several standard and dynamically corrected pocketing geometries are shown in Fig. 6. The conventional pocketing geometries are borrowed from the NC library of a CATIA CAD/CAM system. In conventional pocketing, the tool paths are spaced at equal distances without considering the stability of the milling operation. Here, the tool paths are dynamically corrected with the aid of a stability data bank, and are shown in the same figure. The dynamically corrected tool paths have different axial and radial depth of cuts depending on the direction of cut. The linear tool path geometry (Fig. 6(c)) does not exist in CATIA and has been newly introduced in this work.

A sample procedure for automatic generation of spiral tool paths for a rectangular pocket is shown in Fig. 7. The pocket geometry is part of the overall design, and available in the geometric model database of the CAD/CAM system. In this particular spiral tool path, the directions of the cuts are in the x and y directions, and the corresponding stability table is extracted from the data bank for up- and down-milling operations as shown in Table 2. The cutter starts the cut in a full immersion mode from a corner of the pocket; thus the width of cut is equal to the diameter of the cutter, i.e. $a_e = D$. From Table 2, the corresponding stable axial depth of cut, $b = 3.5$ mm, is selected for both the x and y directions. The pocket boundary, represented by tool path {1,2,3,4,1} are milled at $b = 3.5$-mm increments until the bottom of the pocket is reached. In short, the pocket wall is completely finished first. The remaining metal

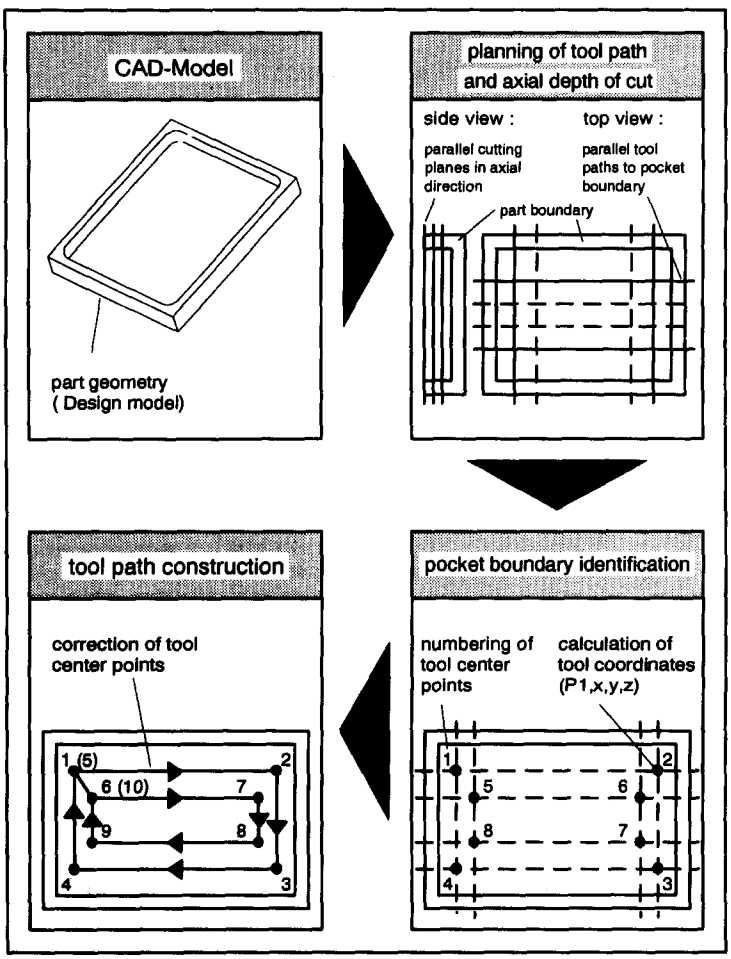

FIG. 7. Automatic generation of the tool path on a CAD/CAM system.

TABLE 2. CRITICAL DEPTH AND WIDTH OF CUTS

Down-milling		Axial depth of cut b (mm) Direction + X	+ Y
Radial depth of cut a_e	0.2 D	8.0	12.0
	0.3 D	7.1	6.0
	0.4 D	6.8	5.5
	0.5 D	6.4	5.0
	0.6 D	6.0	4.7
	0.7 D	5.5	4.3
	0.8 D	5.1	4.0
	0.9 D	4.2	3.7
	1.0 D	3.5	3.5

Up-milling		Axial depth of cut b (mm) Direction + X	+ Y
Radial depth of cut a_e	0.2 D	7.2	16.1
	0.3 D	5.1	13.6
	0.4 D	4.3	11.4
	0.5 D	4.1	9.5
	0.6 D	3.9	7.3
	0.7 D	3.7	6.2
	0.8 D	3.6	5.3
	0.9 D	3.5	4.1
	1.0 D	3.5	3.5

is removed as optimally as possible from the stability table. For example, if the longest feed direction is x, the combination of axial depth $b = 5.1$ mm and radial width $a_e = 0.8D$ in the down-milling mode produces the largest allowable material removal rate without chatter. The axial depth of cut is kept constant, and the corresponding maximum radial width of the cuts are selected in the x and y directions during the remainder of the pocketing process. The tool path coordinates are automatically calculated by simply drawing lines parallel to the pocket walls with offsets equal to the radial width of the cuts, and the heights are calculated from the chatter-free axial depth of the cuts. A similar algorithmic procedure is followed in zigzag and linear tool paths for removing the excess metal island in the pocket. In all three tool path types, the walls of the pocket are always finished first in the full immersion mode. In the zigzag tool path (Figure 6(b)), the cutter alternates between the up- and down-milling; thus appropriate radial width of cuts are selected from the stability table (i.e. Tables 1 and 2) depending on the feed direction. In the newly introduced linear tool path, the tool always cuts in one direction (x or y). The cutter retracts at the end of each cutting cycle, and it is rapidly positioned to the beginning of the next tool path segment.

The procedure outlined above is programmed into a CATIA CAD/CAM system via its graphical user application interface. Similar to the standard interactive generation of NC programs in pocketing, the pocket boundary is selected with the aid of a mouse on the graphic station. The tool number, material and cutting speed are selected by the user. According to the procedure outlined above, the chatter-free tool path is automatically calculated by the interfaced program, which selects the axial depth and radial width of cuts from the stability data bank pointed by the tool number and workpiece.

The advantages of the proposed tool path generation method are compared for the same tool, machine and workpiece material as given before. The pocket size of the test workpiece is $180 \times 110 \times 20$ mm^3. First, the tool path for a pocket is generated using the available standard routines in the CATIA system. Chatter-free axial depth

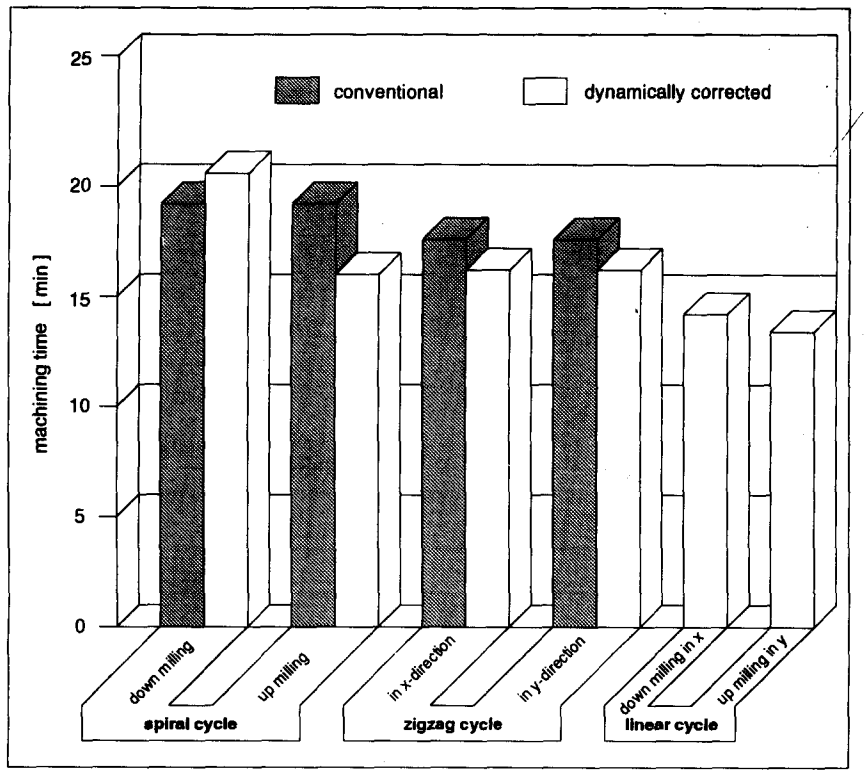

FIG. 8. Comparison of conventionally and dynamically corrected machining time.

of cuts are selected by the user for a full immersion case, and the radial widths are scheduled by the CATIA's pocketing routines. Later, the tool path for the same pocket is automatically generated with the aid of the stability data bank where the optimal chatter-free axial and radial width of cuts are stored. The machining times for the spiral, zigzag and linear tool paths for the up- and down-milling modes are calculated and compared in Fig. 8. The table indicates that the machining time is shortest when the pocket is machined by the newly introduced linear tool path routine assisted by the stability data bank. The conventional tool paths, even though a realistic chatter-free constant axial depth of cut is selected, give a larger machining time than the dynamically corrected paths.

4. CONCLUSION

A method for chatter-free NC tool path generation in CAD/CAM systems is presented. It is assumed that the cutting stiffness for the workpiece material and the transfer functions of the machine tool with an attached end mill are experimentally measured. The stability data bank is prepared by time domain simulations of chatter in end milling. The maximum chatter-free axial and radial width of cuts are identified for each cutting speed, and stored in the CAD/CAM system's NC database. The radial width and axial width of cuts are automatically generated for pocketing operations during NC program preparation. The method is shown to machine pockets efficiently without chatter vibrations.

REFERENCES

[1] S. A. TOBIAS, *Schwingungen an Werkzeugmaschinen*. Carl Hanser, München (1961).
[2] J. TLUSTY, Dynamics of high speed milling, *Trans. ASME J. Engng Ind.* **108**, 59–67 (1986).
[3] M. WECK, E. VERHAAG and M. GATHER, Adaptive control for face-milling operations with strategies for avoiding chatter-vibrations and for automatic cut distribution, *Ann. CIRP* **24**, (1975).
[4] M. WECK and K. TEIPEL, *Dynamisches Verhalten spanender Werkzeugmaschinen*. Springer, Berlin (1987).

[5] Y. ALTINTAS and P. CHAN, In-process detection and suppression of chatter in milling, *Int. J. Mach. Tools Manufact.* **32**, 329–347 (1992).
[6] S. SMITH and J. TLUSTY, Stabilizing chatter by automatic spindle speed regulation, *Ann. CIRP* **41**, 433–436 (1992).
[7] J. TLUSTY and F. ISMAIL, Basic non-linearity in machining chatter, *Ann. CIRP* **30**, (1981).
[8] D. MONTGOMERY and Y. ALTINTAS, Mechanism of cutting force and surface generation in dynamic milling, *Trans. ASME J. Engng Ind.* **113**, 161–168 (1991).
[9] M. WECK, W. KÖNIG, C. BEER and J. LAUSCHER, Assimilation of a common CAD/CAP-system into dies and molds manufacturing, *Computer-Aided-Design and Manufacture of Dies and Molds*, Chicago (1988).
[10] Y. ALTINTAS and A. SPENCE, End milling force algorithms for CAD systems, *Ann. CIRP* **40**, 31–34 (1991).
[11] J. TLUSTY and S. SMITH, NC-programming for quality in milling, *Proc. 16th NAMRC*, SME (1988).
[12] J. TLUSTY, S. SMITH and C. ZAMUDIO, New NC-routines for quality in milling, *Ann. CIRP* **39**, 517–521 (1990).
[13] M. WECK, C. BEER and R. GNOYKE, Erhöhung der Prozeßstabilität durch ungleichgeteilte Werkzeuge, Strategien zur Werkzeugauslegung, *VDI Z.* **133**, 64–70 (1991).
[14] M. WECK and C. BEER, Entwicklung eines Verfahrens zur Simulation des statischen und dynamischen Prozeßverhaltens beim Fräsen und dessen Anwendung bei der NC-Programmierung, Abschlußbericht zum Forschungsvorhaben S 214, Stiftung Industrieforschung (1992).
[15] P. VAN LOON, Modal parameters of mechanical structures, Doctoral thesis, KU Leuven, Belgium (1974).